

# Quadruply Bonded Mo<sub>2</sub> Molecules: An Emitter-Resonator Integrated Quantum System in Free Space

Miao Meng, Ying Ning Tan, Zi Cong He, Zi Hao Zhong, Jia Zhou, Yu Li Zhou, Guang Yuan Zhu, Chun Y. Liu\*

Department of Chemistry, College of Chemistry and Materials Science, Jinan University, 601 Huang-Pu Avenue West, Guangzhou 510632, China

\* Correspondence: tcyliu@jnu.edu.cn

*Dedicated to the discovery of metal–metal quadruple bonds by F. Albert Cotton 60 years ago*

## Abstract

In recent decades, significant progress has been made in construction and study of individual quantum systems consisting of the basic single matter and energy particles, i.e., atoms and photons, which show great potentials in quantum computation and communication.<sup>1</sup> Here, we demonstrate that the quadruply-bonded Mo<sub>2</sub> unit of the complex can trap photons of visible light under ambient conditions, producing intense local electromagnetic (EM) field that features squeezed states,<sup>2</sup> photon antibunching,<sup>3</sup> and vacuum Rabi splitting.<sup>4</sup> Our results show that both the electronic and vibrational states of the Mo<sub>2</sub> molecule are modified by coherent coupling with the scattered photons of the Mo<sub>2</sub> unit, as evidenced by the Rabi doublet<sup>4</sup> and the Mollow triplet<sup>5</sup> in the incoherent resonance fluorescence and the Raman spectra. The Mo<sub>2</sub> molecule, acting as an independent emitter-resonator integrated quantum system, allows optical experiments to be conducted in free space, enabling fundamental quantum phenomena to be observed through conventional spectroscopic instrumentation. This provides a new platform for study of field effects and quantum electrodynamics (QED) in the optical domain. The insights gained from this study advance our understanding in metal-metal bond chemistry, molecular physics and quantum optics, with applications in quantum information processing, optoelectronic devices and control of chemical reactivity.

## Introduction

To achieve the coherent coupling between atoms and photons, it is necessary to confine one of the two components in a small area, commonly referred to as a “box”,<sup>1</sup> and then introduce the other under precise control of optical physical parameters, including the number of atoms and photons. Quantum optical experiments have long faced significant challenges in both instrumentation and operational techniques. For instance, in the Wineland’s ion trapping experiments, individual ions are confined at a cryogenic temperatures using laser cooling techniques,<sup>1,6,7,8</sup> while in the Haroche’s photon box experiments,<sup>1,9,10</sup> the Rydberg atoms with the main quantum number as high as 50 are prepared to interact with photons in a micromaser. In these controlled environments, where perturbations are minimized, atomic transitions interact coherently with oscillating EM fields, allowing the generation of exciton-polaritons—quasi-Bose-Einstein particles that combine the characters of both atoms and photons. The eigenstates of such hybrid systems are typically described by the Jaynes-Cummings Hamiltonian,<sup>11,12,13</sup> which models the resonant coupling between a two-level atom and a single photonic mode at the individual atom-photon level.

In order to reduce the photonic mode volume  $V$  and thus increase the field amplitude for strong matter-light interactions,<sup>1,4</sup> various plasmonic cavities with two nanoparticles spaced by a nanometer gap have been intensively studied over the past decades.<sup>14</sup> Using the nanoparticle-on-the-mirror (NPOM) technique, the size of the gold sphere has approached the atomic scale and the effective mode volume is reduced to  $10^{-2} \text{ nm}^3$ .<sup>15</sup> Studies in quantum optics indicate that when the interfacial gap ( $d$ ) of a metallic sphere dimer is further reduced to the contact region ( $d \leq 0$ ), tip-to-tip charge transfer (CT) occurs *via* quantum tunneling,<sup>16</sup> generating the scattered EM field that is useful for driving a light-matter interaction in the visible region. Recent theoretical and experimental advances have led us to investigate the quantum optical responses of dinuclear transition complex molecules with a  $\text{Mo}_2$  (ref. 17) or  $\text{Ni}_2$  (ref. 18) core, where the metal-metal separation falls in the quantum tunneling regime. Spectroscopic results showed that the electronic transitions in the  $\text{Mo}_2$  complexes are

split and shifted, revealing the formation of the exciton-polaritons in cavity-free solution.<sup>17</sup> In-depth study on the Ni<sub>2</sub> complex demonstrated that the collective coupling of  $N$ -molecule ensembles scales as  $N\sqrt{N}\Omega$ ,<sup>18</sup> which significantly differs from the  $\sqrt{N}\Omega$  scaling in the Tavis-Cummings model.<sup>19</sup> The M<sub>2</sub> quantum system enables unprecedented control over quantum optical phenomena at the molecular level, achieving field quantization without a cavity.<sup>10</sup> In particular, the quadruply bonded Mo<sub>2</sub> unit with the interfacial distance  $d < 0$  becomes a desirable testbed for exploring the limit of quantum optical effects,<sup>16</sup> with the potential to construct the practical ultrascale qubit in quantum circuits.

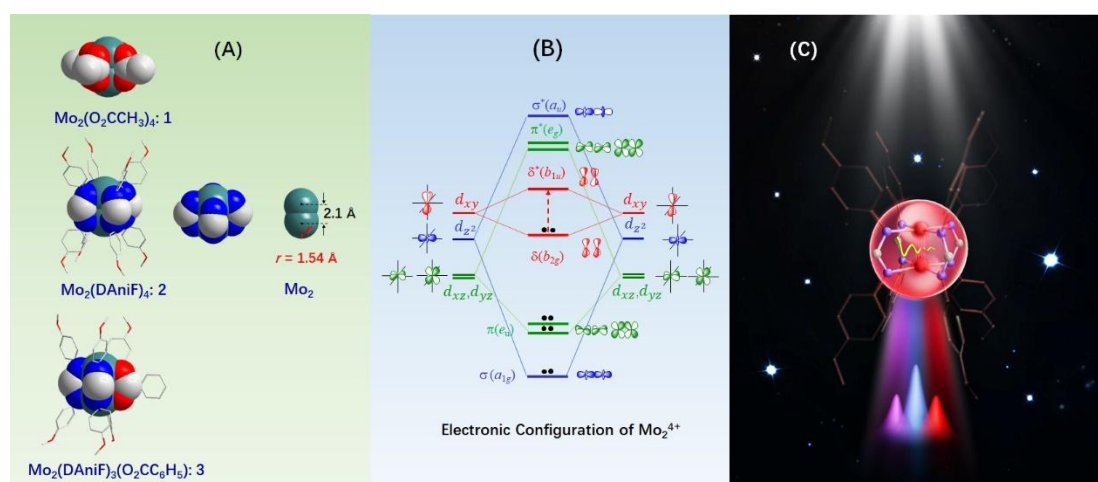


**Figure 1. The molecular structure, electronic configuration, and resonant optical coupling of the Mo<sub>2</sub> complexes.** (A) Space-filling models for Mo<sub>2</sub>(O<sub>2</sub>CCH<sub>3</sub>)<sub>4</sub> (**1**), Mo<sub>2</sub>(form)<sub>4</sub> (**2** and **2'**) and Mo<sub>2</sub>(DAniF)<sub>3</sub>(O<sub>2</sub>CC<sub>6</sub>H<sub>5</sub>) (**3**). (B) The electronic configuration of σ<sup>2</sup>π<sup>4</sup>δ<sup>2</sup> for a quadruply bonded Mo<sub>2</sub> unit. (C) Illustration of the evolution of the Mollow triplet fluorescence in the Mo<sub>2</sub> molecular system (**2**).

In 1964, a *Science* paper by F. Albert Cotton<sup>20</sup> elucidated the molecular structure of Re<sub>2</sub>Cl<sub>8</sub><sup>2-</sup> in terms of Pauling's valence bond theory, which recognizes the quadruple bonds between the two rhenium (III) atoms in the molecule and pioneered the dimetal coordination chemistry.<sup>21</sup> The formation of quadruple bonds between the two transition metal ions removes the degeneracy of the atomic orbitals, resulting in an electronic σ<sup>2</sup>π<sup>4</sup>δ<sup>2</sup> configuration for the M<sub>2</sub> center, as shown in Figure 1B. In the σ<sup>2</sup>π<sup>4</sup>δ<sup>2</sup>

scheme, the  $\delta$  orbital is the highest occupied molecular orbital (HOMO) of the  $M_2$  unit, and the  $\delta^*$  orbital becomes the lowest unoccupied molecular orbital (LUMO).<sup>21</sup> This energy diagram endows a quadruply bonded dimetal complex with the metal-based close shell ground state and the characteristic electric dipole and spin allowed  $\delta$  ( $b_{2g}$ ) $\rightarrow\delta^*(b_{1u})$  (HOMO to LUMO) transition, i.e., the  $A_{1g} \rightarrow A_{2u}$  transition for the  $M_2$  molecules under  $D_{4h}$  symmetry.  $Mo_2$  molecules typically have a paddlewheel geometry, with  $Mo_2(O_2CCH_3)_4$  being the prototype shaped as a Chinese lantern (Figure 1A).

However, some  $Mo_2$  complexes exhibit unusual spectroscopic properties that cannot be understood from their electronic structures. For example, for  $Mo_2(TiPB)_4$ , where  $TiPB = 2,4,6$ -triisopropylphenyl carboxylate,<sup>22</sup> the characteristic  $\delta \rightarrow \delta^*$  transition, expected to appear at  $\sim 440$  nm, is not visible in the absorption spectrum, whereas the singly oxidized  $[Mo_2(TiPB)_4]^+$  shows an intense absorption band at 550 nm that cannot be explained by the  $\sigma^2\pi^4\delta^2$  scheme. In our study of the photoinduced electron transfer (ET) in the donor ( $Mo_2$ )-bridge-acceptor ( $Mo_2$ ) complexes,<sup>23</sup> anomalous ET kinetics were obtained from the ultrafast transient spectroscopic study, showing that the donor-acceptor ET is faster than the charge recombination from the bridge to the  $Mo_2$  center by an order of magnitude. Furthermore, the phenylene-bridged  $Mo_2$  dimers<sup>24</sup> exhibit the intervalence charge transfer (IVCT) bands in the infrared (IR) region, i.e.,  $4800-2450\text{ cm}^{-1}$ , whereas the pyrazine-bridged diruthenium mixed-valence complex, known as the Cruetz-Taube ion, exhibits the IVCT band at  $6410\text{ cm}^{-1}$  in the near-IR region.<sup>25</sup> The exceptionally low energy Frank-Condon barrier for long-range intramolecular electron transfer in the  $Mo_2$  dimers suggests an energy gain by coherent coupling of the molecule with light.<sup>17</sup>

In this work, we have investigated four  $Mo_2$  complexes in terms of light-matter interaction, including  $Mo_2(O_2CCH_3)_4$  (**1**),  $Mo_2(DAniF)_4$  (**2**) ( $DAniF = N, N'$ -di(*p*-anisyl)formamidinate),  $Mo_2(DTolF)_4$  (**2'**) ( $DTolF = N, N'$ -di(*p*-tolyl)formamidinate), and  $Mo_2(DAniF)_3(O_2CC_6H_5)$  (**3**) (Figure 1A, Figures S1, S2, S3 and S4)). In previous work,<sup>26,27,28</sup> the molecular and electronic structures and UV-visible spectra of **1**, **2**, **2'**

and the singly oxidized  $[2']^+$  were studied from a pure chemical perspective. Complexes **2** ( $2^+$ ) and **3** ( $3^+$ ) were included in our primary study of the molecule-photon interaction in the  $\text{Mo}_2$  molecular systems.<sup>17</sup> These molecules exhibit a paddlewheel structure for the coordination shell with the two Mo atoms separated by 0.21 nm and  $d = -0.1 \text{ nm} < 0$  (Figure 1A).<sup>17,27,28</sup> The two  $\text{Mo}^{2+}$  ions in the  $\text{Mo}_2^{4+}$  unit are about 0.04 nm apart, falling in the contact regime.<sup>16</sup>

## Results and Discussion

**Quantum Optical Responses of the  $\text{Mo}_2$  Complexes and Natural Frequency of the  $\text{Mo}_2$  resonator.** Complex **1** exhibits a single broad fluorescence band with a maximum at  $\sim 400 \text{ nm}$  when excited by optical parametric generation (OPG) of a fundamental laser beam with a wavelength  $\lambda_{\text{ex}}$  varying between 560 nm and 700 nm (Figure 2A). This peak does not correspond to the decay of the excited state ( $\delta^*$ ) to the ground state ( $\delta$ ), which occurs at  $\sim 435 \text{ nm}$  ( $23000 \text{ cm}^{-1}$ ),<sup>29</sup> nor does it align with any other defined electronic transition. This fluorescence behavior is similar to what has been observed for  $\text{Cu}_2(\text{O}_2\text{CCH}(\text{C}_2\text{H}_5)(\text{CH}_2)_3\text{CH}_3)_4$  ( $\text{Cu}_2$ )<sup>17</sup> and  $\text{Ni}_2(\text{DAniF})_4$  ( $\text{Ni}_2$ ),<sup>18</sup> both of which have unbound dimetal units and show fluorescence at 420 nm and 380 nm, respectively. We attribute this fluorescence to scattering of the dimetal ( $\text{M}_2$ ) unit upon excitation, analogous to the PCT modes observed in nanoparticle dimers.<sup>14,16</sup> The scattering field around the  $\text{Mo}_2$  center ( $\omega_{\text{Mo}_2}$ ) is extremely intense, primarily due to the Purcell effect, which arises from the atomic-scale confinement of the  $\text{Mo}_2$  unit.<sup>14,16,18</sup> This enhanced local EM field propagates traversing the  $\text{Mo}_2$ – $\text{Mo}_2$  bond axis (Figure 2B), which is represented by a characteristic fluorescence spectrum for different  $\text{M}_2$  nuclearities. The transition energy defines the natural frequency of the  $\text{M}_2$  unit, functioning as a dimetal resonator.<sup>18</sup> For example, the  $\text{Mo}_2$  unit, with the shortest  $\text{M}(\text{II})\cdots\text{M}(\text{II})$  distance (0.04 nm), has a natural frequency (400 nm) falling between  $\text{Ni}_2$  ( $\omega_{\text{Ni}_2} = 380 \text{ nm}$ ,  $d_{\text{Ni}_2} = 0.214 \text{ nm}$ ) and  $\text{Cu}_2$  ( $\omega_{\text{Cu}_2} = 420 \text{ nm}$ ,  $d_{\text{Cu}_2} = 0.118 \text{ nm}$ ). Of the three  $\text{M}_2$  units, the natural frequency varies depending on the  $\text{M}(\text{II})$ – $\text{M}(\text{II})$  distance, following a similar observation for nanoparticle dimers in the quantum

tunneling regime.<sup>16</sup> This suggests a critical distance  $d_{QR} \sim 0.12$  nm for  $M_2$  systems, which is significantly smaller than the  $d_{QR} \approx 0.31$  nm observed in atomic-scale plasmonic cavities.<sup>16</sup> Thus, this fluorescence feature for the  $M_2$  complexes is due to a pure quantum optical effect related to the geometry of the dimetal unit, regardless of the coordination environment influencing the electronic structure. The reduced  $d_{QR}$  for  $M_2$  units and the blue shift of the natural frequency ( $\omega_{M_2}$ ), compared to those for the metal sphere dimers, are attributed to the extremely short M–M distances and the positive charge of the  $M^{2+}$  ion.

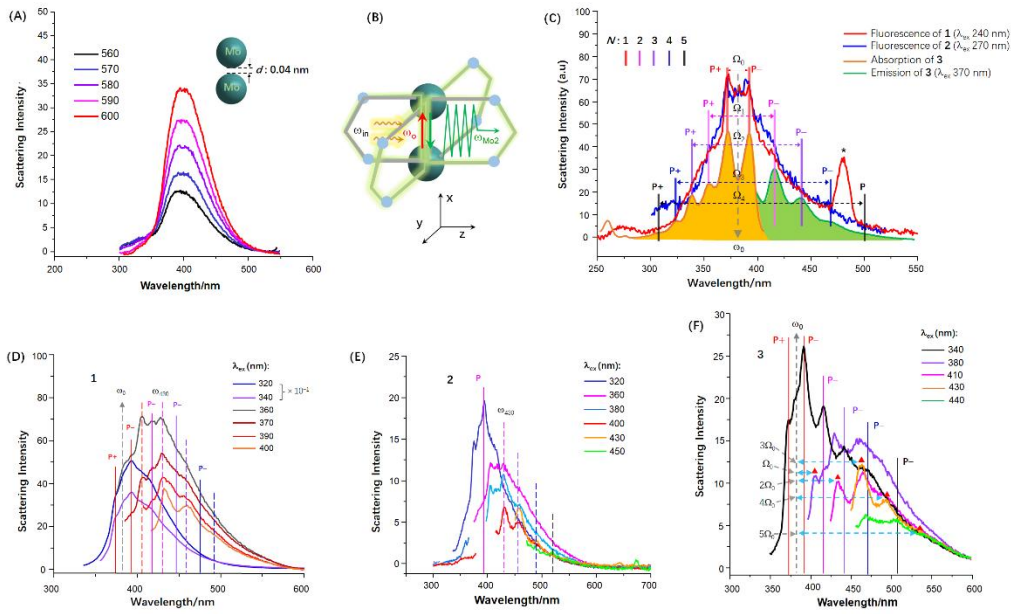


**Figure 2. Quantization of classical visible light by the  $Mo_2$  unit.** (A) Fluorescence of  $Mo_2(O_2CCH_3)_4$  (**1**) showing the thermal-averaged scattering continuum of the  $Mo_2$  unit under incoherent excitation. (B) A pictorial illustration of the conversion of incident classical light ( $\omega_{in}$ ) into quantum light ( $\omega_{Mo_2}$ ) through the  $Mo_2$  unit. (C) Fluorescence spectra of the  $Mo_2$  complexes showing the Rabi doublets for collective coupling for the  $N$ -molecule ensembles. The asterisk peak indicates the double frequency signal of the excitation. (D) Spectral variations of **1** with varying excitations, showing the Mollow triplets derived by exciting the sidebands and their transformation through the Rabi doublet at 417 nm. The colored vertical solid and dashed lines mark the Rabi splitting and the Mollow triplet states, respectively. (E) Featured fluorescence spectra for **2**, showing the ladder structure of the dressed states with progressively lowering the excitation energy. (F) Featured fluorescence

spectra for **3**, showing the transformation of the Rabi states into the Mollow states with excitations of  $\lambda_{\text{ex}} > 380$  nm.

Excitation of **1** and **2** with monochromatic beams of  $\lambda_{\text{ex}} = 240\text{-}270$  nm results in multiple emission peaks symmetrically distributed around the 380 nm position, as shown in Figure 2C. This unusual fluorescence profile has been observed for the Ni<sub>2</sub> analog, Ni<sub>2</sub>(DAniF)<sub>4</sub>, which has been attributed to the vacuum Rabi splitting of the two-level CT mode ( $\omega_0$ ) of Ni<sub>2</sub> resonantly coupled to the scattering field  $\omega_{\text{Ni}_2}$ .<sup>18</sup> In the spectra (Figure 2C), the two peaks at 370 nm and 390 nm centered at  $\omega_0$  (380 nm) are assigned to the exciton-polaritons P<sup>+</sup> and P<sup>-</sup> for the single molecules, giving a coupling rate ( $\Omega_0$ ) of 1380 ( $\pm 10$ ) cm<sup>-1</sup>, nearly identical to that obtained in the Ni<sub>2</sub> system.<sup>18</sup> The symmetrically distributed shoulder bands show the vacuum Rabi splitting of  $\omega_0$  for the collective coupling of the *N*-molecule ensembles ( $N = 2 - 5$ ) through the strong resonant dipole-dipole interactions.<sup>18</sup> The intensity distribution of the spectra reflects the statistical distribution of the *N*-molecule ensembles in the solution, revealing a lower concentration for the higher order (larger *N*) molecular array. The Rabi splitting states for high-order collective coupling,<sup>18</sup> which are not well resolved in incoherent resonance fluorescence, are confirmed by the combined absorption-emission spectra for **3** (Figure 2C).<sup>18</sup> The measured collective coupling rates, 4430 cm<sup>-1</sup> ( $N = 2$ ), 7140 cm<sup>-1</sup> ( $N = 3$ ), 9640 cm<sup>-1</sup> ( $N = 4$ ) and 13000 cm<sup>-1</sup> ( $N = 5$ ) (Table S1), are close to those for the Ni<sub>2</sub> system, confirming the scaling  $N\sqrt{N}\Omega$  for collective coupling that is distinct from that in the Tavis-Cummings mode,<sup>19</sup> indicating a breakdown of the dipole blockade in the two-atom Dicke model.<sup>18,30,31</sup>

The parametric agreement in the incoherent resonance fluorescence between the Mo<sub>2</sub> and Ni<sub>2</sub> systems suggests a common physical origin for the optical events in both the bonded and unbonded M<sub>2</sub> systems. The distinct electronic spectra for the unbonded Ni<sub>2</sub>(DAniF)<sub>4</sub> (ref. 18) and the bonded **1**<sup>26,29</sup> and **2** (**2'**)<sup>27,28</sup> rule out the possibility that this featured fluorescence results from a two-level electronic excitation or a Frenkel exciton of the molecule (emitter) coupled to the scattering field. Instead, it is the M $\leftrightarrow$ M CT mode  $\omega_0$ , analogous to the cavity mode for an optical cavity,<sup>4,12</sup>

that is coupled to the scattering field ( $\omega_{M_2}$ ).<sup>18</sup> Importantly, the highly resembling incoherent resonance fluorescence spectra for these two complexes suggest that the Ni<sub>2</sub> and Mo<sub>2</sub> units share very similar CT resonance energies, despite their substantial geometric and coordinative differences. It appears that  $\omega_0 = 26300 \text{ cm}^{-1}$  (380 nm) represents the quantum limit for the M<sub>2</sub> units in the conductive contact regime ( $d_{QR} \geq d \leq 0 \text{ nm}$ ).

**Transition from the Rabi Splitting States to the Mollow Triplet States.** Complex 1 exhibits distinct fluorescence profiles with a gradual decrease of the excitation energy to  $\lambda_{ex} = 400 \text{ nm}$ , as shown in Figure 2D. The spectra reveal Rabi doublets and Mollow triplets for collective coupling of different orders, with transition energies confirming the state transitions observed across M<sub>2</sub> systems.<sup>18</sup> Notably, while similar transitions have been observed in the Ni<sub>2</sub> system,<sup>18</sup> the Mo<sub>2</sub> complex demonstrates key distinctions in its resonant coupling dynamics. An intense triplet structure is observed at 392 nm ( $\omega_{392}$ ) upon excitation at 320 nm and 340 nm, indicating a Mollow triplet that is substantially modified by the squeezed scattering field.<sup>18,31,32,33,34</sup> This Mollow triplet at 392 nm results from excitation of the red Rabi sideband (P<sup>-</sup>) for the single molecules (Figure 2C),<sup>35</sup> highlighting the field-driven state transitions governed by photon antibunching effects and the squeezed states.<sup>18,32,34,36</sup> This  $\omega_{392}$  triplet for the Mo<sub>2</sub> system,<sup>17</sup> which was not observed for the Ni<sub>2</sub> system,<sup>18</sup> results from the enhanced excitation-photon interaction due to better frequency matching between the  $\omega_{392}$  sideband and  $\omega_{Mo_2}$  ( $\sim 400 \text{ nm}$ ). When the excitation wavelength exceeds 370 nm, a new triplet appears with a central peak at 430 nm, corresponding to the second low-energy sideband of the Mollow triplet at resonance, i.e.,  $\omega_{430} = (\omega_0 - 2\Omega_0)$ , which emerges from the resonant coupling of two simultaneously driven molecules.<sup>18,33,34</sup>

The spectrum at 360 nm excitation shows the transition between the Mollow triplets at  $\omega_{392}$  and  $\omega_{430}$  through the Rabi splitting states centered at 417 nm. The  $\omega_{417}$  resonance corresponds to the P<sup>-</sup> Rabi line for the first-order collective coupling (Figure 2C) as well as the red sideband of the  $\omega_{392}$  Mollow triplet (Figure 2D). The



associated polaritons appear at 405 nm (P+) and 430 nm (P-) with a separation of  $1430 \text{ cm}^{-1}$  corresponding to the coupling constant ( $\Omega_0$ ). These results demonstrate that photon antibunching of the Mollow triplet sidebands enable exciting polaritons, as predicted theoretically.<sup>35</sup> This transition between the Rabi splitting states and the Mollow triplet implies a phase-sensitive population decay, a characteristic observed across the  $M_2$  systems,<sup>18</sup> demonstrating the influence of squeezed scattering fields in breaking down the dipole blockade in the two-atom Dicke model.<sup>30,31,32,34,37</sup> Note that in this  $Mo_2$  system, the  $\omega_0$  Mollow triplet is not observed (Figure 2D), while in the  $Ni_2$  system it is extremely weak.<sup>18</sup> These results confirm that the exciton-field interaction is driven by photon antibunching<sup>18</sup> which is diminished at the resonance by strong dipole-dipole interactions between two simultaneously driven molecules.<sup>33,34</sup> For **2**, an intense Mollow triplet with a central peak at 392 nm in Lorentzian lineshape is observed by incoherent excitation at 320 nm (Figure 2E),<sup>17</sup> due to excitation of the  $\omega_{392}$  sideband (Figure 2C). This triplet is transformed into the 430 nm Mollow triplet through the Rabi states when excited at  $\lambda_{ex} = 400 \text{ nm}$ , in agreement with the observations for complex **1**. The fluorescence spectra of **2** indicate that field quantization by  $Mo_2$  provides the lowest energy quantum light with a wavelength of 522 nm when excited at 450 nm (Figure 2E), confirming the results obtained for the  $Ni_2$  system.<sup>18</sup>

For complex **3**, excitation at 340 nm allows observation of the low-energy half of the full Rabi splitting spectrum of collective coupling, which exhibits five P-branches for the  $N$ -molecule ensembles ( $N = 1 - 5$ ) (Figure 2F), consistent with the results shown in Figure 2C. The energies of these peaks are predicted by  $\omega_0 - (N\sqrt{N} \Omega_0)/2$ , which satisfies the collective coupling scaling  $N\sqrt{N} \Omega_0$ .<sup>18</sup> This Rabi spectral profile is transformed into the Mollow multiplet structure at 430 nm with the near-resonance excitation (380 nm). By gradually lowering the excitation energy, five peaks are probed at 404 nm, 430 nm, 460 nm, 492 nm and 530 nm with an energy interval of  $1450 (\pm 50) \text{ cm}^{-1}$  (Figure 2F, red triangles). These peaks correspond to the valleys in the spectrum at 340 nm excitation, indicating a phase difference of  $\pi$

between the Rabi and Mollow states.<sup>18</sup> The transition energies are scaled by  $(\omega_0 - N\Omega_0')$  ( $N = 1, 2, 3, 4$  and  $5$ ) with  $\Omega_0' = 1450 \text{ cm}^{-1}$ , which is reasonably larger than the  $\Omega_0$  determined from the Rabi doublet for the single molecules.<sup>18</sup> These results demonstrate that the additional sidebands result from collective coupling of the  $N$ -molecule ensembles through strong dipole-dipole interactions, and thus, share the same physical origin as the multiple Rabi components.

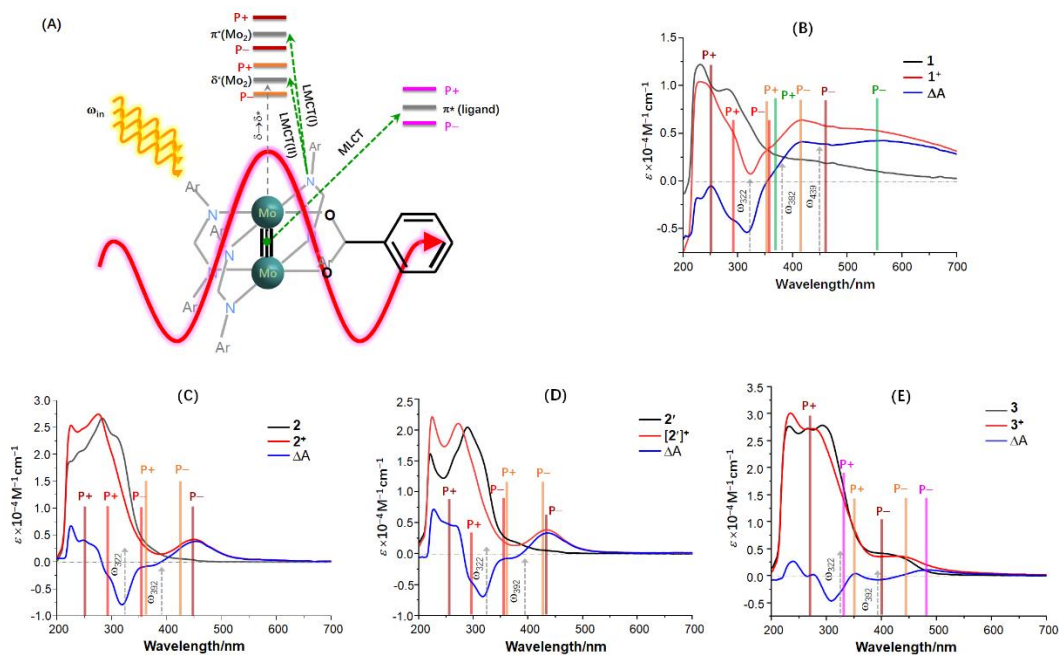


**Figure 3. Vacuum Rabi splitting of the electronic transitions in UV-Vis absorption spectra for the singly oxidized Mo<sub>2</sub> complexes.** (A) Resonant coupling of the two-level transitions with the quantized local scattering field in the singly oxidized Mo<sub>2</sub> formamidinates. (B), (C), (D) and (E) The UV-Vis spectra for **1** (**1<sup>+</sup>**), **2** (**2<sup>+</sup>**), **2'** (**[2']<sup>+</sup>**) and **3** (**3<sup>+</sup>**), respectively, and the corresponding  $\Delta A$  spectra. The gray vertical dashed lines with an upper arrow indicate the field oscillating modes ( $\omega_{\perp}$ ). The Rabi sidebands P+ and P- of different excitations are marked by colored vertical lines: red (dark red) for excitation I, orange for excitation II, green for excitation III, and pink for the MLCT excitation.

### Vacuum Rabi Splitting of the Electronic Transitions in the Cationic Complexes.

Under the  $D_{4h}$  ligand field symmetry, the theoretical studies of **1** (ref.26) and the computational model of **2** and **2'**, Mo<sub>2</sub>[(NH)<sub>2</sub>CH]<sub>4</sub>,<sup>27</sup> produced essentially the same molecular orbital (MO) diagrams, revealing similar electronic transitions related to

the Mo<sub>2</sub> center. Experimentally, three bands around 320 nm, 390 nm and 440 nm, designated I, II and III, respectively, are found for each of these Mo<sub>2</sub> complexes,<sup>26,27,28,29</sup> and are of particular interest. After some controversy in the assignment of these absorptions in earlier studies,<sup>26,29,38,39</sup> it is now generally accepted that I and II are assigned to the 1a<sub>u</sub> (O or N) → 5e<sub>g</sub> (π\*) and 4e<sub>g</sub> (O or N) → 2b<sub>1u</sub> (δ\*) transitions,<sup>27,28</sup> respectively, while the lowest energy absorption is attributed to the δ(2b<sub>2g</sub>) → δ\*(2b<sub>1u</sub>) transition or III.<sup>27,28,29,39</sup> These transitions are all dipole-allowed. Transitions I and II involve the atomic orbitals of the ligand donors (O or N) in the ground state and the Mo<sub>2</sub>-based antibonding orbitals π\* or δ\* in the excited state (Figure 1B), thus belonging to the ligand to metal charge transfer (LMCT) transitions (Figure 3A). In the spectra for the neutral complexes in solution (Figures 3B-3E), the transitions are weak and overlapping, especially for III, which prevents an accurate determination of the transition energies.

The singly oxidized cationic species show intense absorptions that differ significantly from the spectra of the neutral precursors (Figures 3B-3E). This cannot be explained by the electronic structure alone, because theoretical calculations of **2** and **2**<sup>+</sup> showed similar MO diagrams and comparable transition energies for the neutral and oxidized molecules.<sup>27</sup> For each complex, the spectral differences between the neutral and cationic complexes are manifested in the difference spectrum (ΔA),<sup>17</sup> which is derived by subtracting the molar extinction coefficients of the neutral complex from those of the oxidized complex over the spectral region (Figures 3B-3E). In general, the cationic complex shows more intense and more absorptions,<sup>17</sup> compared to the neutral complex, which accounts for the dark color of the compounds.<sup>27</sup> In the ΔA spectra, all complexes show a pronounced spectral valley at ~ 320 nm, corresponding to transition I in energy. For the Mo<sub>2</sub> formamidinates **2**, **2'** and **3**, the negative absorptions at ~ 390 nm in the ΔA spectra coincide with band II. The disappearance of the characteristic bands I and II and the appearance of new intense absorptions appearing around the resonances are reminiscent of the optical coupling of the two-level excitations occurring in the cationic species.<sup>17</sup> This optical coupling

switches the normal excitation mode to “dark”, developing a composite system consisting of the two-level molecule coupled at resonance to a single populated mode of the scattering field, as proposed in the earlier theoretical study.<sup>40</sup> In this context, we interpret the absorption spectra of the positively charged molecules in terms of vacuum Rabi splitting of the electronic transitions.<sup>4</sup>

Discrete quantum lights of wavelengths 322 nm, 382nm and 392 nm are found in the spectrum of the quantized scattering field (Figure 2C), which correspond remarkably well to the absorptions I and II, respectively. For the cationic species, the electronic transitions are resonantly or near-resonantly coupled to the vacuum field of the single modes, evolving the P<sup>+</sup> and P<sup>-</sup> exciton polaritons. In the spectrum of **1**<sup>+</sup> and the  $\Delta A$  spectrum (Figure 3B), two pairs of absorption bands are symmetrically distributed around the position of  $\omega_{322}$ . The inner pair has two bands at 292 nm (P<sup>+</sup>) and 358 nm (P<sup>-</sup>), separated by 6314 cm<sup>-1</sup>. The 250 nm peak in the  $\Delta A$  spectrum marks the P<sup>+</sup> component for the second pair, with the P<sup>-</sup> band located at 452 nm, taking into account the resonant coupling of the 320 nm transition (I) with  $\omega_{322}$  and the intense absorption in the expected region. Thus, the outer pair has the P<sup>+</sup> and P<sup>-</sup> branches separated by 17876 cm<sup>-1</sup> (2.2 eV). Taking the separation of 6314 cm<sup>-1</sup> for the absorptions of the first pair as the coupling strength for the normal mode I of the single molecule ( $\Omega_0$ ), the measured coupling strength of 17876 cm<sup>-1</sup> for the second pair is in remarkable agreement with the first-order collective coupling constant for the  $N = 2$  ensemble when scaled as  $N\sqrt{N}\Omega_0$ ,<sup>18</sup> i.e.,  $2\sqrt{2}\Omega_0 = 17860$  cm<sup>-1</sup>. The primary and the collective coupling of excitation I to  $\omega_{322}$  is confirmed by systems **2**<sup>+</sup> (Figure 3C) and [**2'**]<sup>+</sup> (Figure 3D) with similar  $\Delta A$  profiles, both with similar coupling strengths (Table S2).

The resonant coupling of excitation II with the  $\omega_{392}$  light mode is indicated by the shallow spectral valleys at 392 nm for the three Mo<sub>2</sub> formamidinate complexes. For **2**<sup>+</sup> and [**2'**]<sup>+</sup>, the P<sup>+</sup> is located at ~363 nm, overlapping with the first P<sup>-</sup> of I and forming the 350-365 nm absorption plateau in the  $\Delta A$  spectra (Figures 3C and 3D). For both, the P<sup>-</sup> is located at ~ 427 nm, closely overlapping with the second P<sup>-</sup> of I

and giving rise to the pronounced asymmetric absorption at  $\sim 450$  nm that is absent for the neutral molecules. The relatively low energy of the second P– band of I for  $\mathbf{2}^+$ , compared to that for  $[\mathbf{2}']^+$ , is consistent with the lower transition energy of I for  $\mathbf{2}$  due to the stronger electron-donating of the anisyl groups of DAniF.<sup>28</sup> This assignment of the dominant absorption to the polaritonic transitions is justified by the increased dipole moment ( $\Delta\mu$ ) for the LMCT transitions (I and II) for the cationic complex, which directly increases the oscillation strength ( $f_{os}$ ) of the excitation and thus, enhances the exciton-photon interaction. In contrast, the assignments to the electronic transitions at resonance in the traditional chemical sense (e.g., N ( $4e_g$ )  $\rightarrow \delta^*$  ( $2b_{1u}$ ))<sup>27</sup> do not explain the largely shifted absorptions and the increased intensity for the cationic species because the low  $f_{os}$  for the oxidized molecule would decrease the absorption intensity. Furthermore, the neutral molecule  $\mathbf{2}'$  shows this II band at 375 nm as a faint shoulder,<sup>28</sup> distanced from the 434 nm band for  $[\mathbf{2}']^+$  by  $3625\text{ cm}^{-1}$ . This large redshift of the absorption can be perfectly explained by the vacuum Rabi splitting of the resonance, but not by the electronic transition.<sup>27</sup> The transition II for  $\mathbf{1}$ , which cannot be identified in the spectrum (Figure 3B), is expected to have a higher transition energy than those for the formamidinate analogs due to the substitution of the O donors for the N donors. Indeed, the O  $\rightarrow \delta^*$  transition energy was calculated to be 3.71 eV or 334 nm.<sup>26</sup> Consequently, for  $\mathbf{1}^+$ , this excitation is coupled to the higher energy mode  $\omega_{382}$ , rather than  $\omega_{392}$ , as evidenced by the absence of the 392 nm valley in the  $\Delta A$  spectrum (Figure 3B). Resonant coupling of II with  $\omega_{382}$  in  $\mathbf{1}^+$  is further supported by the P– band at 416 nm and the notable shoulder band at 353 nm for the P+ in the spectrum, giving a coupling rate of  $4300\text{ cm}^{-1}$ , similar to that of  $\mathbf{2}^+$  and  $[\mathbf{2}']^+$  (Table S3).

The spectrum of  $\mathbf{3}$  (Figure 3E) shows a broad absorption from 380 to 480 nm, which involves three transitions: II ( $\sim 390$  nm), MLCT (395 nm), and III (446 nm).<sup>17</sup> For  $\mathbf{3}^+$ , the absorption extends to 500 nm upon single oxidation. This extension is likely due to the additional two-level excitation, i.e., the MLCT which occurs at 395 nm (Figure 3A). Optical coupling is the only way to observe a low energy signal for

the high energy excitation. Therefore, the P<sup>-</sup> band of the MLCT transition can be unambiguously located at 483 nm, which has been probed at the same wavelength by the femtosecond transient and fluorescence spectra,<sup>17</sup> and thus, the P<sup>+</sup> branch is located at 330 nm from the resonant coupling to the  $\omega_{392}$  mode (Figure 3E). The presence of the 330 nm polariton is evidenced by the blue shift and reduction of the I valley in the  $\Delta A$  spectrum compared to the  $\Delta A$  spectra for **2** and **2'**. The coupling strength for the MLCT excitation is determined to be 9600 cm<sup>-1</sup> (1.2 eV) and the normalized coupling rate  $\eta = 0.19$  in the ultrastrong regime. This ultrastrong coupling is obviously due to the large MLCT transition dipole moment (Figure 3A). The broad negative absorption at 392 nm in the  $\Delta A$  spectrum is attributed to the bleaching of the II and MLCT excitations as a result of the resonant coupling of these two electronic normal modes with the photonic  $\omega_{392}$  mode. For excitation II, the polariton components are located at 350 nm (P<sup>+</sup>) and 445 nm (P<sup>-</sup>) (Figure 3E). This P<sup>-</sup> transition contributes significantly to the dominant absorption for the cationic species, as observed for the other three systems. In the 320 nm region, the  $\Delta A$  spectrum shows the familiar funnel-shaped profile, indicating the resonant coupling between excitation I and the field mode  $\omega_{322}$ ; however, for **3**<sup>+</sup>, only one pair of Rabi transitions is probed at 270 nm and ~400 nm, and the coupling is less pronounced.

It is interesting to note that the three oxidized formamidinato Mo<sub>2</sub> complexes **2**<sup>+</sup>, [**2'**]<sup>+</sup> and **3**<sup>+</sup> do not show absorptions that can be attributed to the  $\delta \rightarrow \delta^*$  electronic transition and that result from vacuum Rabi splitting of the excitation (III). The  $\Delta A$  spectra do not show a spectral valley around the 440 nm position corresponding to the vertical transition (III) for the neutral molecules. These results indicate that the  $\delta \rightarrow \delta^*$  transition is not coupled to the scattering field of the Mo<sub>2</sub> unit. In contrast, the oxidized **1**<sup>+</sup> shows a broad absorption ranging from 500 to 650 nm with a maximum at 550 nm and a shallow spectral valley at ~450 nm in the  $\Delta A$  spectrum (Figure 3B), signaling the coherent coupling of III with light. In the study of Mo<sub>2</sub>(TiPB)<sub>4</sub><sup>22</sup> there is no  $\delta \rightarrow \delta^*$  transition observed for the neutral complex, but an intense absorption at 550 nm is observed in the spectrum for the oxidized species [Mo<sub>2</sub>(TiPB)<sub>4</sub>]<sup>+</sup>, accompanied

by a high-energy band at 365 nm. These two bands are centered at 439 nm, corresponding to the position of III. Given the  $\omega_{439}$  mode in the quantized scattering field (Figure 2C), we attribute the two bands to the polaritonic transitions to the P+ and P- states resulting from the resonant coupling of the  $\delta \rightarrow \delta^*$  transition with light. Our interpretation of the anomalous absorption spectra for  $\text{Mo}_2(\text{TiPB})$  is strongly supported by the broad emission with a maximum at 550 nm for  $\text{Mo}_2(\text{O}_2\text{CCF}_3)_4$  at low temperature (1.3 K), which exhibits a vibrational hyperfine structure of the Mo-Mo stretching frequency ( $\omega_v$ ).<sup>38</sup> This long-lived emission does not energetically correspond to an electronic transition, nor does the broad absorption at 550 nm for  $[\text{Mo}_2(\text{TiPB})_4]^+$  and  $[\text{Mo}_2(\text{O}_2\text{CCH}_3)_4]^+$  ( $\mathbf{1}^+$ ), according to the MO calculations.<sup>27</sup> The vibrational structure in the fluorescence transition clearly indicates that this 550 nm emission is due to vertical radiative decay of the excited state with an energy level significantly lower than the  $\delta^*$  state,<sup>26,38,39</sup> which is most likely the P- component of the Rabi doublet of the  $\delta \rightarrow \delta^*$  transition. On this basis, we located the P+ component for  $\mathbf{1}^+$  at 365 nm in the spectrum (Figure 3B), as observed for  $[\text{Mo}_2(\text{TiPB})_4]^+$ . These results reveal coherent coupling between the  $\delta \rightarrow \delta^*$  transition and the scattering field in these carboxylate-supported complexes, demonstrating that the ligand environment plays a role in controlling the electron-photon interaction. Importantly, the optical coupling of the electronic transitions to the scattering field demonstrates that the quantum effects of the  $\text{Mo}_2$  molecule as an individual quantum system can be manipulated by molecular design, which has the potential applications in quantum information processing<sup>6,8</sup> and in the control of chemical reactivity.<sup>8,41</sup>

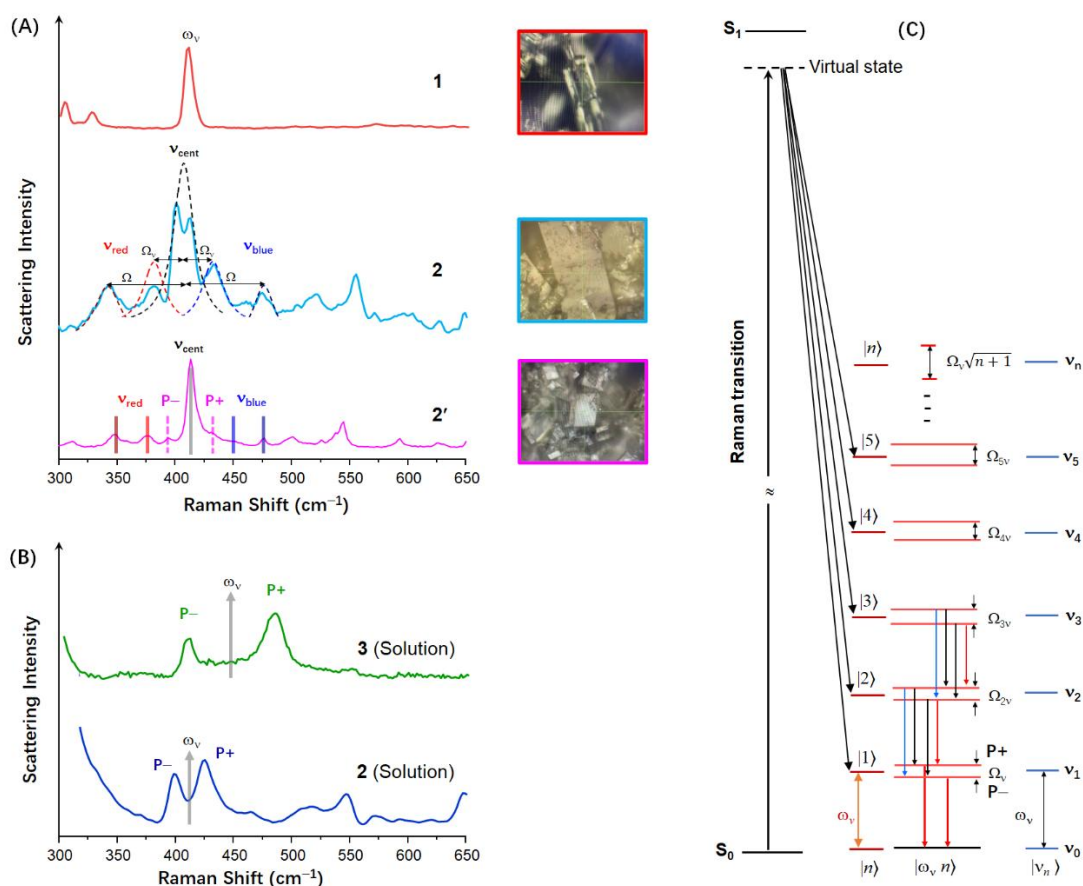


**Figure 4. Vibrational strong coupling for the Mo<sub>2</sub> complexes.** (A) Raman spectra of crystalline samples **1** (top panel), **2** (middle panel) and **2'** (bottom panel). The measurements were performed by focusing a 532 nm laser beam on a single crystal, as shown in the insets. (B) Raman spectra of **2** (bottom panel) and **3** (top panel) in dichloromethane solution. (C) Schematic illustration of the formation of the Rabi doublet and the Mollow triplets of the Mo–Mo stretching mode for **2'** in Raman scattering processes.

**Resonant Coupling of the Mo–Mo Vibrational Mode with Photons Scattered by Mo<sub>2</sub>.** Illumination of a single crystal **1** with a 532 nm laser beam produces an intense single scattering peak at 410 cm<sup>-1</sup> in the Raman spectrum (Figure 4A, top panel), which signals the Mo–Mo stretching mode ( $\omega_v$ ).<sup>26,29,38,39</sup> For crystal **2**, multiple scattering peaks are found symmetrically distributed around the position of  $\omega_v$  (Figure 4A, middle). The intense peak at 407 cm<sup>-1</sup> is split at the tip (Figure S5), indicating the hyperfine structures of  $\omega_v$  due to the presence of the nearly equivalent spin-1/2 states.<sup>6</sup> Ignoring this hyperfine structure, the crystal **2** exhibits a quintet structure with two



pairs of sidebands centered at  $407 \text{ cm}^{-1}$  (Figure 4A, middle panel), indicating resonant coupling of the vibrational mode ( $\omega_v = 407 \text{ cm}^{-1}$ ) to the scattered photons in the two-photon Raman transition (Figure 4C). We consider the first triplet, characterized by  $\nu_{\text{cent}}$  at  $407 \text{ cm}^{-1}$  and its satellites  $\nu_{\text{cent}} \pm 26 \text{ cm}^{-1}$ , to be the primary Mollow triplet<sup>5</sup> due to the population decay of the dressed states of the photon states  $|1\rangle$  and  $|2\rangle$  (Figure 4C), giving a coupling rate of  $26 \text{ cm}^{-1}$  and  $\eta = 0.03$  in the strong coupling regime. The additional sidebands are displaced from  $\nu_{\text{cent}}$  by  $64 \text{ cm}^{-1}$ , i.e.,  $\Omega = 64 \text{ cm}^{-1}$ , resulting from the high-level Fock states  $|n\rangle$  with  $n = 5$  according to  $\Omega = \Omega_0 \sqrt{n+1}$ <sup>7</sup> (Figure 4C, Table S4). Note that both sideband pairs are asymmetric with unequal integrated intensities. For the first pair, the  $\nu_{\text{blue}}$  peak is more intense, while the  $\nu_{\text{red}}$  peak has low intensity. For the second pair, this relative intensity of the  $\nu_{\text{blue}}$  vs.  $\nu_{\text{red}}$  peaks is reversed. This gives the  $\nu_{\text{blue}}$  and  $\nu_{\text{red}}$  peaks similar total integrated intensities, and the two triplets show comparable overall integrated sideband intensities. On this basis, we explain that the asymmetry of the sideband intensity is caused by the undesired population decay between the two scattering domains, corresponding to the Fock states  $|1\rangle$ - $|2\rangle$  and  $|4\rangle$ - $|5\rangle$  (Figure 4C).

In the Raman spectrum of the single crystal **2'** (Figure 4A, bottom panel), the intense peak at  $414 \text{ cm}^{-1}$  represents the Mo-Mo stretching frequency ( $\omega_v$ ) peak, which is higher in energy than that of **2**. There are three pairs of side peaks symmetrically surrounding the  $\omega_v$  peak. The separation between the two peaks of the first pair is similar to the distances of the two peaks of the second pair from the central peak, i.e.,  $\sim 38 \text{ cm}^{-1}$ . This indicates that the two peaks of the first and second pair belong to the Rabi branches P+ and P- and the sidebands of the Mollow triplet of  $\omega_v$ , respectively, which give similar values of the vibrational coupling constant, i.e.,  $\Omega_v \approx 38 \text{ cm}^{-1}$ . This coupling constant is larger than that for **2** ( $26 \text{ cm}^{-1}$ ) presumably due to the high frequency of Mo-Mo stretching. The two peaks of the second pair are displaced from  $\omega_v$  by  $65 \text{ cm}^{-1}$  (Figure 4A, bottom panel, and Table S4), giving  $\Omega = 65 \text{ cm}^{-1}$  for the high-level Mollow triplet, characterized by  $\omega_v$  and  $\omega_v \pm \Omega$ . This coupling strength for the second Mollow triplet indicates that the corresponding corresponding dressed

states result from coupling  $\omega_v$  with the Fock state  $|2\rangle$  based on  $\Omega = \Omega_0 \sqrt{n+1}$ <sup>7</sup> (Figure 4C, Table S4). Therefore, the first and second Mollow triplets are attributed to the scattering of the dressed state manifolds involving two adjacent Fock states  $|1\rangle$ - $|2\rangle$  and  $|2\rangle$ - $|3\rangle$ , respectively, with relatively low population of the high-level states as indicated by the spectral asymmetry. To the best of our knowledge, up to date, a vibration-polariton Mollow triplet has not been observed experimentally, although vacuum Rabi splitting of a vibrational mode by zero EM field in an infrared cavity has recently been demonstrated.<sup>42</sup> Remarkably, the Mo<sub>2</sub> systems **2** and **2'**, through its characteristic Mo–Mo stretching mode, allows the first observation of the Jaynes-Cummings ladder structure for the dressed vibrational states.<sup>13</sup>

For **2** in solution, where the molecules are randomly oriented and freely moving, the Raman spectrum (Figure 4B, bottom panel) shows two isolated peaks at 400 cm<sup>-1</sup> and 425 cm<sup>-1</sup> centered at 412.5 cm<sup>-1</sup>. These two peaks are assigned to the vibration-polaritons P+ and P– resulting from the vacuum Rabi splitting of  $\omega_v$ <sup>42</sup> in the two-photon Raman transition (Figure 4C). The resonant coupling of  $\omega_v$  to the scattered photons gives rise to a vibrational coupling rate ( $\Omega_v$ ) of 25 cm<sup>-1</sup>, similar to the coupling constant for the crystal **2** (Table S4). The vibrational coupling properties of **2** are further confirmed by the Raman scattering of the powder sample, which shows the combined scattering features of the single crystal and the solution (Figure S6). Complex **3** in solution exhibits the Rabi doublet consisting of the P+ at 410 cm<sup>-1</sup> and the P– at 484 cm<sup>-1</sup> (Figure 4B, top panel), indicating a  $\omega_v$  of 447 cm<sup>-1</sup>. The large blue shift of  $\omega_v$  and the increased  $\Omega_v$  (74 cm<sup>-1</sup>), compared to that of **1**, **2** and **2'**, can be attributed to the coordination of the electron-withdrawing carboxylate group in **3**. The observation of the Mollow triplet and the Rabi doublet of the Mo–Mo stretching mode indicates the strong resonant coupling of the vibrational state with the scattering field that is greatly enhanced by the atomistic confinement,<sup>15</sup> analogous to the optical coupling of the electronic transitions observed in this Mo<sub>2</sub> molecular system. The distinctive scattering spectrum profiles for the complexes in crystal and solution, which yield similar coupling constants, imply that in both cases, the vibrational coupling

occurs at the single molecule level, reflecting the nature of the Mo<sub>2</sub> system as a Jaynes-Cummings molecule.

## **Conclusion**

Sixty years after the discovery of multiple bonds between metal atoms by F. A. Cotton, this study demonstrates that single Mo<sub>2</sub> complex molecules can trap visible light photons between the quadruply bonded Mo atoms, generating an extremely strong local field of quantum light across a broad spectrum of discrete single modes. With these chemical entities containing a Mo<sub>2</sub> unit, we are able to observe the behavior of individual quantum systems composed of a single electron and a single photon at the single-molecule level in free space under ambient conditions, exploring the quantum-classical boundary. Spectral analyses reveal that the quantized scattering field of the Mo<sub>2</sub> unit enables driving the electronic and vibrational coupling of the molecule with light, profoundly modifying the electronic and vibrational structures. The light-matter interaction establishes an efficient energy exchange between the molecule and the external light source through the quadruply bonded Mo<sub>2</sub> unit, which is of particular fundamental and technological importance.<sup>1,6,8,41</sup>

## **Acknowledgments**

We acknowledge the primary financial support from the National Natural Science Foundation of China (22171107, 21971088, 21371074), Natural Science Foundation of Guangdong Province (2018A030313894), Jinan University, and the Fundamental Research Funds for the Central Universities.

## **Author Contribution**

C.Y.L. conceived this project and designed the experiments and worked on the manuscript. M.M. carried out the major experimental work, including chemical synthesis, data collection and analysis, and prepared the Supplementary Information.

Y.N.T., Z.C.H. involved in the spectroscopic data analysis and assisted in manuscript preparation. Z.H.Z., Y.L.Z., J.Z., G.Y.Z. were involved in experimental investigations.

**Competing interests:** The authors declare no conflict of interest.

## References

---

- <sup>1</sup> Serge Haroche, Jean-Michel Raimond Exploring the Quantum Atoms, Cavities and Photons. Oxford University Press (2006).
- <sup>2</sup> Walls, D. F. Squeezed states of light. *Nature*, 306, 141–146 (1983).
- <sup>3</sup> Kimble, H. J., Dagenais, M. & Mandel, L. Photon antibunching in resonance fluorescence. *Phys. Rev. Lett.* 39, 691 (1977).
- <sup>4</sup> Thompson, R. J., Rempe, G. & Kimble, H. J. Observation of Normal-Mode Splitting for an Atom in an Optical Cavity. *Phys. Rev. Lett.* 68, 1132 (1992).
- <sup>5</sup> Mollow, B. R. Power spectrum of light scattered by two-level systems. *Phys. Rev.* 188, 1969–1975 (1969).
- <sup>6</sup> Monroe, C., Meekhof, D. M., King, B. E., Itano, W. M. & Wineland, D. J. Demonstration of a Fundamental Quantum Logic Gate. *Phys. Rev. Lett.* 75, 4714 (1995).
- <sup>7</sup> Meekhof, D. M., Monroe, C., King, B. E., Itano, W. M., & Wineland, D. J. Generation of Nonclassical Motional States of a Trapped Atom. *Phys. Rev. Lett.* 76, 1796 (1996).
- <sup>8</sup> Blatt, R., Wineland, D. Entangled states of trapped atomic ions. *Nature* 453, 1008–1015 (2008).
- <sup>9</sup> Gleyzes, S., Kuhr, S., Guerlin, C., Bernu, J., Deléglise, S., Busk Hoff, U., Brune, M., Raimond, J. M. & Haroche, S. Quantum Jumps of Light Recording the Birth and Death of a Photon in a Cavity. *Nature* 446, 297–300 (2007).
- <sup>10</sup> Brune M, Schmidt-Kaler F, Maali A, et al. Quantum Rabi oscillation: A direct test of field quantization in a cavity. *Phys. Rev. Lett.*, 76, 1800 (1996).
- <sup>11</sup> Jaynes, E. T. & Cummings, F. W. Comparison of quantum and semiclassical radiation theories with application to the beam maser. *Proc. IEEE.* 51, 89–109 (1963).

- 
- <sup>12</sup> Alsing, P., Guo, D.-S. & Carmichael, H. J. Dynamic Stark effect for the Jaynes-Cummings system. *Phys. Rev. A* 45, 5135–5143 (1992).
- <sup>13</sup> Fink, J. M. et al. Climbing the Jaynes-Cummings ladder and observing its  $\sqrt{n}$  nonlinearity in a cavity QED system. *Nature* 454, 315–318 (2008).
- <sup>14</sup> Chikkaraddy, R. et al. Single-molecule strong coupling at room temperature in plasmonic nanocavities. *Nature* 535, 127–130 (2016).
- <sup>15</sup> Benz, F. et al. Single-molecule optomechanics in “picocavities”. *Science* 354, 726–729 (2016).
- <sup>16</sup> Savage, K. J. et al. Revealing the quantum regime in tunnelling plasmonics. *Nature* 491, 574–577 (2012).
- <sup>17</sup> Tan, Y. N. et al. Zero-dimensional molecular exciton-polaritons in cavity-free solutions, *Cell Rep. Phys. Sci.*, 4, 101342 (2023).
- <sup>18</sup> Meng, M., Tan, Y. N., He, Z. C., Zhong, Z. H., Zhou, J., Zhou, Y. L., Zhu, G. Y., Liu, C. Y. Quantization of Visible Light by a Ni<sub>2</sub> Optical Resonator. Submitted, (2024).
- <sup>19</sup> Tavis, M. & Cummings, F. W. Exact solution for an N-molecule-radiation-field Hamiltonian. *Phys. Rev.* 170, 379 (1968).
- <sup>20</sup> Cotton, F. A. et al. Mononuclear and polynuclear chemistry of rhenium (III): Its pronounced homophilicity. *Science*, 145, 1305–1307 (1964).
- <sup>21</sup> Cotton, F. A., Murillo, C. A. & Walton, R. A. *Multiple Bonds Between Metal Atoms*, 3rd ed. Springer Science + Business Media, Inc.: New York. 2005.
- <sup>22</sup> Cotton, F. A., Daniels, L. M., Hillard, E. A. & Murillo, C. A. Filling a void: Isolation and characterization of tetracarboxylato dimolybdenum cations. *Inorg. Chem.*, 41, 1639-1644 (2002).
- <sup>23</sup> Cheng, T. et al. Photoinduced  $\delta$  electron transfer in phenylene bridged Mo<sub>2</sub> dimers. *Phys. Chem. Chem. Phys.*, 19, 1740–1745 (2017).
- <sup>24</sup> Zhu, G. Y. et al. Crossover between the adiabatic and nonadiabatic electron transfer limits in the Landau-Zener model. *Nat. Commun.*, 12, 456 (2021).
- <sup>25</sup> Creutz, C.; Taube, H. J. *Am. Chem. Soc.*, 91, 3988–3989 (1969).
- <sup>26</sup> Norman, J. G., Kolari, H. J., Gray, H. B. & Trogler, W. C. Electronic structure of

---

dimolybdenum tetraformate, dimolybdenum (4+) ion, and dimolybdenum. *Inorg. Chem.*, 16, 987–993(1977).

<sup>27</sup> Cotton, F. A., Feng, X. & Matusz, M. Experimental and theoretical study of tetrakis (di-*p*-tolylformamidinato) dimolybdenum and  $[\text{Mo}_2(\text{form})_4]^+(\text{form}^-=[(\text{p-tol})\text{NCHN}(\text{p-tol})])^-$ . *Inorg. Chem.*, 28, 594–601 (1989).

<sup>28</sup> Lin, C., Protasiewicz, J. D., Smith, E. T. & Ren, T. Linear free energy relationships in dinuclear compounds. 2. Inductive redox tuning via remote substituents in quadruply bonded dimolybdenum compounds. *Inorg. Chem.*, 35, 6422–6428 (1996).

<sup>29</sup> Martin, D. S., Newman, R. A. & Fanwick, P. E. Polarized electronic absorption spectra for dimolybdenum (II) tetraacetate. *Inorg. Chem.*, 18, 2511–2520 (1979).

<sup>30</sup> Dicke, R. H. Coherence in Spontaneous Radiation Processes. *Phys. Rev.* 93, 99–110 (1954).

<sup>31</sup> Palma, G. M. & Knight, P. L. Phase-sensitive population decay: The two-atom Dicke model in a broadband squeezed vacuum. *Phys. Rev. A* 39, 1962–1969 (1989).

<sup>32</sup> Carmichael, H. J., Lane, A. S. & Walls, D. F. Resonance fluorescence from an atom in a squeezed vacuum. *Phys. Rev. Lett.*, 58, 2539 (1987).

<sup>33</sup> Griffin, R. D. & Harris, S. M. Two-atom resonance fluorescence including the dipole-dipole interaction. *Phys. Rev. A* 25, 1528 (1982).

<sup>34</sup> Ficek, Z. & Sanders, B. C. Two-atom resonance fluorescence spectrum in a squeezed vacuum including the dipole-dipole interaction. *Quantum Opt.* 2, 269–286 (1990).

<sup>35</sup> Carreño, J. C. L., Muñoz, C. S., Sanvitto, D., Valle, E. d. & Laussy, F. P. Exciting polaritons with quantum light. *Phys. Rev. Lett.*, 115, 196402 (2015).

<sup>36</sup> Meystre, P. & Zubairy, M. S. Squeezed states in the Jaynes-Cummings model. *Phys. Lett. A*, 89, 390–392 (1982).

<sup>37</sup> Agarwal, G. S., Narducci, L. M. & Apostolidis, E. Effects of dispersion forces in optical resonance phenomena. *Opt. Commun.*, 36, 285–290 (1981).

<sup>38</sup> Trogler, W. C., Solomon, E. I., Trajberg, I. B., Ballhausen, C. J. & Gray, H. B. Studies of the polarization behavior, temperature dependence, and vibronic structure of the 23,000-cm<sup>-1</sup> absorption system in the electronic spectra of tetrakis [ $\mu$ -(acetato-O, O')] dimolybdenum (Mo-Mo) and related compounds. Emission spectrum of tetrakis [ $\mu$ -(trifluoroacetato-O, O')] dimolybdenum (Mo-Mo) at 1.3 K. *Inorg. Chem.*, 16, 828–836 (1977).

---

<sup>39</sup> Bino, A., Cotton, F. A. & Fanwick, P. E. Crystal structure and polarized, low-temperature electronic absorption spectrum of tetrakis (L-leucine) dimolybdenum (II) dichloride bis (p-toluenesulfonate) dihydrate. *Inorg. Chem.*, 19, 1215–1221 (1980).

<sup>40</sup> Carmichael, H. J. & Walls, D. F. Proposal for the measurement of the resonant Stark effect by photon correlation techniques. *J. Phys. B: Atom. Mol. Phys.* 9, L43 (1976).

<sup>41</sup> Garcia-Vidal, F. J., Ciuti, C. & Ebbesen, T. W. Manipulating matter by strong coupling to vacuum fields. *Science* 373, eabd0336 (2021).

<sup>42</sup> Shalabney, A., George, J., Hutchison, J. A., Pupillo, G., Genet, C., Ebbesen, T. W. Coherent coupling of molecular resonators with a microcavity mode. *Nat. Commun.* 2015, 6, 5981.